ADVANCES IN ATMOSPHERIC SCIENCES, VOL. 35, FEBRUARY 2018, 182–194

• **Original Paper** •

Study of Aerosol Direct and Indirect Effects and Auto-conversion Processes over the West African Monsoon Region Using a Regional Climate Model

Zeinab SALAH*[1], Ahmed SHALABY[1], Allison L. STEINER[2], Ashraf S. ZAKEY[1], Ritesh GAUTAM[3,5], and Mohamed M. ABDEL WAHAB[4]

[1]*The Egyptian Meteorological Authority, Cairo* 11784*, Egypt*

[2]*University of Michigan, Department of Climate and Space Sciences and Engineering, Ann Arbor, MI* 48109-2143*, USA*

[3]*Centre of Studies in Resources Engineering and Interdisciplinary Program in Climate Studies, Indian Institute of Technology Bombay, Bombay* 400076*, India*

[4]*Cairo University, Department of Astronomy, Space Science and Meteorology, Giza* 12613*, Egypt*

[5]*Environmental Defense Fund, Washington DC* 20009*, USA*

(Received 7 April 2017; revised 30 July 2017; accepted 5 September 2017)

ABSTRACT

This study assesses the direct and indirect effects of natural and anthropogenic aerosols (e.g., black carbon and sulfate) over West and Central Africa during the West African monsoon (WAM) period (June–July–August). We investigate the impacts of aerosols on the amount of cloudiness, the influences on the precipitation efficiency of clouds, and the associated radiative forcing (direct and indirect). Our study includes the implementation of three new formulations of auto-conversion parameterization [namely, the Beheng (BH), Tripoli and Cotton (TC) and Liu and Daum (R6) schemes] in RegCM4.4.1, besides the default model's auto-conversion scheme (Kessler). Among the new schemes, BH reduces the precipitation wet bias by more than 50% over West Africa and achieves a bias reduction of around 25% over Central Africa. Results from detailed sensitivity experiments suggest a significant path forward in terms of addressing the long-standing issue of the characteristic wet bias in RegCM. In terms of aerosol-induced radiative forcing, the impact of the various schemes is found to vary considerably (ranging from −5 to −25 W m^{-2}).

Key words: aerosol, cloud, West African monsoon, auto-conversion, RegCM

Citation: Salah, Z., A. Shalaby, A. L. Steiner, A. S. Zakey, R. Gautam, and M. M. Abdel Wahab, 2018: Study of aerosol direct and indirect effects and auto-conversion processes over the West African monsoon region using a regional climate model. *Adv. Atmos. Sci.*, **35**(2), 182–194, https://doi.org/10.1007/s00376-017-7077-3.

1. Introduction

The large uncertainty in the assessment of aerosol–cloud–radiation interactions poses a significant challenge toward better constraining climate sensitivity (IPCC, 2013). An improved quantification of these interactions is necessary for a better understanding of past and future climate change. Changes in the concentrations and properties of aerosols alter the Earth's climate, since aerosols scatter and/or absorb sunlight and directly affect the climate by modifying the radiant energy distribution in the surface–atmosphere system. Furthermore, through their critical role as cloud condensation nuclei and ice nuclei, aerosols can indirectly modify cloud properties (e.g., Costantino and Bréon, 2013; Fan et al., 2016). Increasing aerosol concentrations due to anthropogenic activities can lead to enhanced cloud droplet number concentrations with smaller radii, enhancing the cloud albedo (first indirect or cloud albedo effect) (Twomey, 1977). As the cloud droplets become smaller, the precipitation efficiency decreases, consequently increasing cloud lifetime and fractional cloud cover (second indirect or cloud lifetime effect) (Albrecht, 1989). In addition, absorbing aerosols such as black carbon (BC) and some organic aerosols can induce radiative heating, leading to modifications of atmospheric stability, cloud cover, and convection strength, i.e., the so called semi-direct effect (Gu et al., 2006, 2012). The simulations of these different effects of aerosols in climate models strongly depend on their emission, mass, composition and size distribution (Seinfeld and Pandis, 2006), as well as the mixing state of the particles (internal or external mixtures), and the parameterization of nucleation processes in the models (Kodros et al., 2015).

The sign and magnitude of different aerosol effects have

* Corresponding author: Zeinab SALAH
Email: zeinabsalah@gmail.com

strong regional dependence (Kodros et al., 2015). Aerosol effects in the West Africa region are complex due to the large diversity of aerosol composition (and sources), including naturally occurring desert dust, marine aerosols, anthropogenic aerosols from urban areas, as well as biomass burning. Mineral dust from the Sahara and biomass-burning particles from Equatorial and Central Africa are frequently transported to the West African monsoon (WAM) region (Chiapello et al., 2005), which ranges from 5°N to 20°N and 10°W to 20°E. Therefore, it is critical toward an improved representation of the complexity of aerosols in this region to carry out in-depth studies of the effects of the various aerosol types, especially in an effort to improve their representation and role in regional aerosol–chemistry–climate model simulations.

Using satellite observations of aerosol and cloud properties from simultaneous MODIS and CALIOP measurements, Costantino and Bréon (2013) showed that aerosols affect cloud microphysics by decreasing the cloud droplet radius and cloud liquid water path (CLWP). They hypothesized that the observed reduction in CLWP is a consequence of dry air entrainment near the cloud top. Using MODIS aerosol products and TRMM precipitation data, Huang et al. (2009) studied the relationship/feedbacks between African aerosols and precipitation during the WAM. They suggested that both dust and smoke contribute to precipitation suppression, with the dust effect evident over the Gulf of Guinea and the smoke effect evident over both land and ocean.

The relative roles of direct and indirect effects of aerosols on the WAM are still poorly characterized; therefore, high-resolution studies, such as regional climate model simulations, can be useful for understanding the processes that drive cloud–aerosol interactions in the region. For example, using RegCM, several studies have used parameterized aerosol indirect effects to understand these processes over eastern Asia (Qian and Giorgi, 1999; Huang, 2005; and Huang et al., 2007), involving different auto-conversion parameterizations. While these simulations did not use a full cloud microphysical treatment, the auto-conversion parameterization was a computationally efficient way to represent the formation of raindrops by collision and coalescence of cloud drops.

As discussed in the aforementioned studies, the direct radiative effect of aerosols could potentially contribute to the suppression of precipitation in the WAM region; however, from the microphysical point of view, the semi-direct and indirect effects have been suggested to play a dominant role toward precipitation suppression (Huang et al., 2009). Therefore, in the present study, we implement different parameterizations of the aerosol indirect effects within RegCM4.4.1 to investigate their impacts on cloud microphysics and precipitation over tropical Africa during the WAM season. In addition, RegCM suffers from a long-standing wet bias problem (relative to CRU, ERA-Interim and TRMM data), as documented in multiple studies of the West Africa and Sahel regions (Sylla et al., 2010; Giorgi et al., 2012; Ji et al., 2016). The overarching aim of our study is to determine the extent to which the implementation of a new auto-conversion scheme, involving the first and second indirect effects, might reduce this wet bias in RegCM.

A description of RegCM4.4.1 and the simulation experiments is provided in section 2. Section 3 discusses the direct effect, as well as the first and second indirect aerosol effects, using three different auto-conversion parameterizations, over the western and central parts of the African domain. In section 4, we present a summary of the results and draw some conclusions from the key findings.

2. Model description and experimental design

The regional climate model used in this work (RegCM4.4.1) is a hydrostatic model with sigma vertical levels that can be used to simulate long-term climate (Giorgi et al., 2012). The radiative transfer processes are parameterized using CCM3 (Kiehl et al., 1996). The representation of cloud optical/microphysical properties in RegCM depends on three parameters of cloud: (1) CLWP, which is prognostically calculated by RegCM; (2) cloud cover fraction, which is calculated diagnostically as a function of relative humidity; and (3) cloud droplet effective radius (r_e), defined as the ratio of the third to the second moment of the size spectrum. For convective precipitation, the Grell (1993) scheme is used in the implementation of Giorgi et al. (1993) with Fritsch–Chappell closure (Fritsch and Chappell, 1980). Nonconvective clouds and precipitation are based on the Subgrid Explicit Moisture Scheme (SUBEX) (Pal et al., 2000). The Biosphere–Atmosphere Transfer Scheme (Dickinson et al., 1993) is used for land surface processes, and the scheme of Holtslag (Holtslag et al., 1990) represents boundary layer processes.

The simulations presented here use the RegCM aerosol scheme based on a simplified treatment of sulfur dioxide (SO_2), sulfate (SO_4^{2-}), organic carbon (OC) and BC, which exist as hydrophobic and hydrophilic components, and are treated as externally mixed. The emission fluxes of SO_2, BC and OC are fed directly into the model from the global emissions inventories. The wet deposition of the aerosols is based on the parameterizations of large-scale (Giorgi, 1989) and convective precipitation (Giorgi and Chameides, 1986); in this scheme, the aerosols are not released by evaporation of raindrops. The dry removal depends on fixed dry deposition velocities for each tracer over land and ocean. The scattering and absorption of solar radiation are included based on the aerosol optical properties as described in Solmon et al. (2006).

2.1. *First indirect effect in RegCM4.4*

In RegCM4.4.1, all aerosols have only direct effects on the climate, except SO_4^{2-}, which has direct and first indirect effects. The optical properties of the clouds depend on the r_e, which is calculated as a function of temperature and the type of liquid-phase cloud (e.g., maritime versus continental) (Giorgi et al., 2012). To represent the first indirect effect, r_e (μm) is represented as a function of cloud droplet number concentration (N_c; cm^{-3}), as in the formula of Martin et al. (1994) [Eq. (1)], which is related to the total mass mixing ra-

tio of SO_4^{2-} using the empirical relationship derived by Hegg (1994) [Eq. (2)]:

$$r_e = \left(\frac{3w_L}{4\pi\rho_w k N_c}\right)^{\frac{1}{3}} , \quad (1)$$

$$N_c = 10^6[90.7(10^9\rho_a x_{tot})^{0.45} + 23]\rho_w , \quad (2)$$

where ρ_a and ρ_w are the densities of air and water, respectively (kg m^{-3}); x_{tot} is the mass mixing ratio of total aerosols (kg kg^{-1}); w_L is liquid water content (kg m^{-3}); and $k = 0.80$ for maritime air masses and 0.67 for continental air masses. Although the above parameterization is for SO_4^{2-} aerosol, we assume it is equally applicable to hydrophilic BC and OC as well. This parameterization has been tested in RegCM previously by Qian and Giorgi (1999) and Huang et al. (2007).

2.2. *Implementation of the second indirect effect in RegCM4.4.1*

To represent the aerosol second indirect effect in RegCM4.4.1, the parameterization of cloud microphysics in the model is altered so that the rate of precipitation is affected by the aerosol concentration. In RegCM4.4.1, SUBEX (Pal et al., 2000) calculates the cloud cover fraction based on the relative humidity. In the cloud fraction, a Kessler-type bulk formulation (Kessler, 1969) is used to parameterize the auto-conversion and accretion processes. The Kessler-type formula ("KS" scheme) assumes that precipitation is formed at any model level when the cloud water mixing ratio ($q_L = w_L/\rho_a$) exceeds the threshold value ($q_{L,th}$), as in the following relation:

$$P = C_{ppt}\left(\frac{q_L}{f_c} - q_{L,th}\right) f_c , \quad (3)$$

where P is the rain drop formation rate (kg kg^{-1} s^{-1}), $1/C_{ppt}$ is the characteristic time for which cloud droplets are converted into raindrops, and f_c is the cloud fraction. The threshold value is obtained as a function of temperature according to the following relation derived by Gultepe and Isaac (1997):

$$q_{L,th} = C_{acs}10^{-0.49+0.013T} , \quad (4)$$

where T is temperature in °C, and C_{acs} is the auto-conversion scale factor. Also, in SUBEX (Pal et al., 2000), the amount of accreted cloud water (P_{acc}) and evaporated precipitation (P_{evap}) are expressed as follows:

$$P_{acc} = C_{acc}q_L P_{sum} , \quad (5)$$

$$P_{evap} = C_{evap}(1 - RH)P_{sum}^{\frac{1}{2}} , \quad (6)$$

where C_{acc} is the accretion rate coefficient, P_{sum} is the accumulated precipitation from above falling through the cloud, and C_{evap} is the evaporation rate coefficient.

Several prior studies have found that the second indirect effect is very sensitive to the parameterizations of auto-conversion and cloud cover in models (Lohmann and Feichter, 1997; and Huang et al., 2007). Here, we implement three different auto-conversion schemes in RegCM4.4.1:

The first parameterization depends on Beheng (1994) (referred to as the "BH" scheme), which is based on Lohmann and Feichter (1997):

$$P = \frac{6\times10^{28}\gamma_1 n^{-1.7}(10^{-6}N_c)^{-3.3}(10^{-3}\rho_a q_L/f_c)^{4.7}}{\rho_a} , \quad (7)$$

where $\gamma_1 = 150$ is a tunable parameter, and $n = 10$ is the width parameter of the initial cloud droplet spectrum. All parameters are in SI units.

The second parameterization depends on Tripoli and Cotton (1980) (referred to as the "TC" scheme):

$$P = \frac{0.104 g E_c \rho_a^{\frac{4}{3}} q_L^{\frac{7}{3}}}{\mu(N_c\rho_w)^{\frac{1}{3}}} H(N_{c20} - 10^3) , \quad (8)$$

where g is gravity, $E_c = 0.55$ is the collision/collection efficiency of cloud droplets, $\mu = 1.83\times10^{-5}$ kg m^{-1} s^{-1} is the dynamic viscosity of the air, and H is the Heaviside function. Since cloud droplets convert to rain drops when the N_c of larger than 20 μm in radius (N_{c20}) is more than the 10^3 m^{-3} (Rogers and Yau, 1989), where

$$H = \begin{cases} 1, & N_{c20} > 10^3 \\ 0, & N_{c20} \leqslant 10^3, \end{cases} \quad (9)$$

N_{c20} is calculated assuming a gamma cloud droplet size distribution according to the Khrgian and Mazin distribution (Pruppacher and Klett, 1997).

The third parameterization of auto-conversion (referred to as the "R6" scheme), based on Liu et al. (2004), accounts for the dispersion effect of cloud droplets (Liu et al., 2004, 2007):

$$P = \left(\frac{3}{4\pi\rho_w}\right)^2 \frac{k_2\beta_6^6}{N_c} w_L^3 H(R_6 - R_{6c}) , \quad (10)$$

where R_6 is the mean radius of the sixth moment of the droplet size distributions in Rotstayn and Liu (2005), $k_2 = 1.9\times10^{11}$ cm^{-3} s^{-1} is a constant describing the increase in the collection efficiency of cloud droplets with increasing collector drop size, β_6 represents the dispersion effect of cloud droplets assuming a gamma distribution for the cloud-droplet spectrum,

$$\beta_6 = \left[\frac{(1+3\in^2)(1+4\in^2)(1+5\in^2)}{(1+\in^2)(1+2\in^2)}\right]^{\frac{1}{6}} , \quad (11)$$

and R_{6c} is the critical radius in μm,

$$R_{6c} = 4.09\times10^{-4}\beta_{con}^{\frac{1}{6}}\frac{N_c^{\frac{1}{6}}}{w_L^{\frac{1}{3}}} , \quad (12)$$

where $\in = 1 - 0.7\exp(-\alpha N_c)$, is the relative dispersion of the droplet size distribution, $\alpha = 0.003$ (Rotstayn and Liu, 2005), w_L is in g m^{-3}, N_c is in cm^{-3}, and $\beta_{con} = 1.15\times10^{23}$ s^{-1} is the mean value of the condensation rate constant.

These three auto-conversion schemes differ in their dependence on the total aerosol mixing ratio (x_{tot}), which relates to the r_e and w_L, as shown in the following proportionalities. These are derived by eliminating N_c with x_{tot} and r_e

using Eqs. (1) and (2) in the raindrop formation rate (P) for the BH [Eq. (7)], TC [Eq. (8)] and R6 [Eq. (10)] schemes:

$$\left.\begin{aligned} &\text{BH}: P \propto w_{\text{L}}^{4.7} x_{\text{tot}}^{-1.5} \propto w_{\text{L}}^{1.4} r_{\text{e}}^{9.9} \\ &\text{TC}: P \propto w_{\text{L}}^{2.3} x_{\text{tot}}^{-0.15} \propto w_{\text{L}}^{2} r_{\text{e}} \\ &\text{R6}: P \propto w_{\text{L}}^{3} x_{\text{tot}}^{-0.45} \propto w_{\text{L}}^{2} r_{\text{e}}^{3} \end{aligned}\right\} \quad (13)$$

The precipitation rates simulated by the KS, BH, TC and R6 auto-conversion schemes, with different values of r_{e} and q_{L} are shown in Figs. 1a and b for r_{e} = 10 and 7.5 μm, which represent large and small cloud droplets, respectively. Because the auto-conversion rates depend on the f_{c} in KS and BH, we show the range of values for two f_{c} values (f_{c} = 1 and f_{c} = 0.5; Figs. 1a and b). The cloud fractional cover has an effective influence on the KS auto-conversion rate at low in-cloud liquid water ($q_{\text{L}} \leqslant 0.6$ g kg^{-1}), where the lower f_{c} (f_{c} = 0.5) increases the auto-conversion rate faster than the one (f_{c} = 1) (Figs. 1a and b). For larger droplets (r_{e} = 10 μm), the auto-conversion rate is enhanced by the BH scheme with more efficiency than TC, R6 and KS, respectively. On the other hand, with smaller cloud droplets (r_{e} = 7.5 μm), the auto-conversion in the BH scheme is faster than in the R6 scheme only at extremely low q_{L} ($\leqslant 0.2$ g kg^{-1}), whereas the precipitation rate produced by TC is more than that of BH at $q_{\text{L}} \geqslant 0.1$ g kg^{-1}.

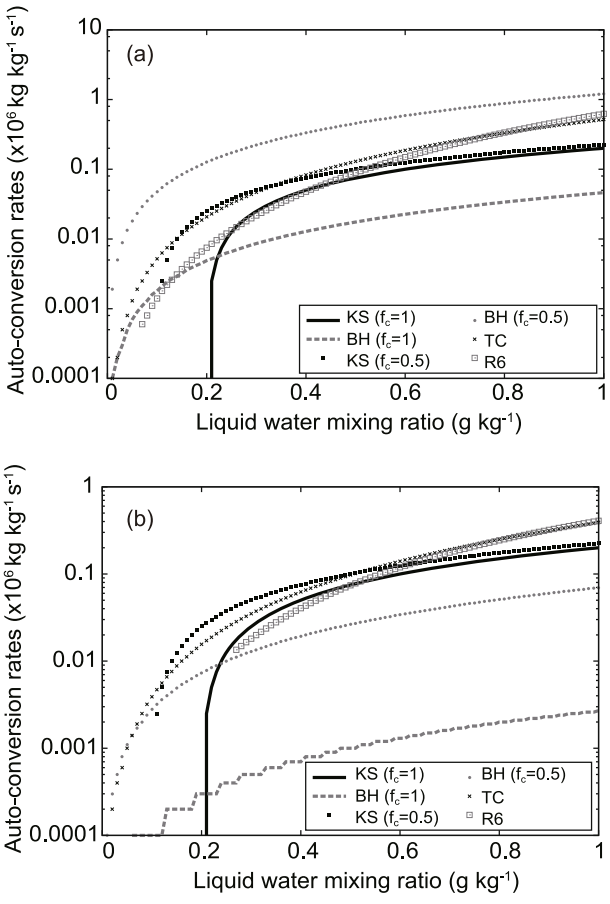

Fig. 1. Auto-conversion rates (P) (units: 10^6 kg kg^{-1} s^{-1}) as a function of liquid water mixing ratio (q_{L}) (units: g kg^{-1}) for the different auto-conversion schemes of KS, BH, TC and R6. The calculations assume an r_{e} of (a) 10 μm and (b) 7.5 μm. Note that for the purpose of these figures, the calculations of the KS and BH schemes assume a cloud fraction cover of f_{c} = 1 and f_{c} = 0.5; KS is unaffected by changing the r_{e}, and its calculation for these figures assumes $q_{\text{L,th}}$ = 0.2 g kg^{-1} in Eq. (3).

2.3. *Experimental design*

The simulations in this study are conducted over a region extending from tropical Africa to northern Africa and the Mediterranean, as shown in Fig. 2. This domain has a complex mixture of aerosols from various origins, such as desert dust, urban pollution and biomass-burning/smoke aerosol. The model domain is centered at (19.0°N, 12.0°E), with a grid of 84 × 116 points at a horizontal grid spacing of 60 km, and 18 vertical sigma levels with the model top at 10 hPa. For our analysis, the region extending from the equator to 15°N is divided into two sub-regions, referred to as the western region (Domain1) and the central region (Domain2), as shown in Fig. 2a. In all simulations, the global data of NCEP-2 provide the meteorological initial and lateral boundary conditions. For the SST, OISSTv2 weekly data are used. For the chemical boundary conditions, we use the global output from the Model for Ozone and Related Chemical Tracers (Emmons et al., 2010). We conduct a one-year simulation (1 October 2005 to 1 December 2006) with the first two months used as model spin-up, and focus on the season of the WAM (June–July–August; JJA).

We simulate online aerosols for the chemical species of SO_4^{2-} and hydrophobic and hydrophilic BC and OC to investigate the effects of the aerosols from biomass and anthropogenic sources. Aerosol emissions are based on the Emission Database for Global Atmospheric Research (EDGAR) (Olivier et al., 2001) for anthropogenic and biomass-burning BC and OC and biogenic SO_2, and the Reanalysis of the Tropospheric Chemical Composition Inventory (RETRO) (Schultz et al., 2007) for anthropogenic SO_2. Figures 2a–c show the spatial distributions of emissions during summer for SO_2, derived from the anthropogenic emissions of RETRO and biomass-burning emissions of EDGAR, and the BC and OC derived from the anthropogenic and biomass-burning emissions of EDGAR. Figure 2a shows that the total emission rates of SO_2 are concentrated around the Mediterranean basin, especially in the large cities due to anthropogenic activities, with emission rates of up to 4×10^{-10} kg m^{-2} s^{-1}. Emissions are also high in West Africa near the Gulf of Guinea, due to biomass burning and anthropogenic activities. The spatial distributions of the total BC emission rates are similar to those of SO_2, as shown in Fig. 2b; the emissions rate reaches 3×10^{-13} kg m^{-2} s^{-1} over the large cities in the Mediterranean and Arabian Peninsula. The emissions of OC (Fig. 2c) follow the same patterns as BC.

To validate and intercompare the simulations, we use gridded (0.5° × 0.5°) observations from the CRU (Mitchell and Jones, 2005) for the monthly surface air temperature and precipitation data over land. The Level-3 (version 5) global-gridded 1° × 1° data product retrieved from MODIS onboard Terra is used to evaluate the total cloud cover distribution over

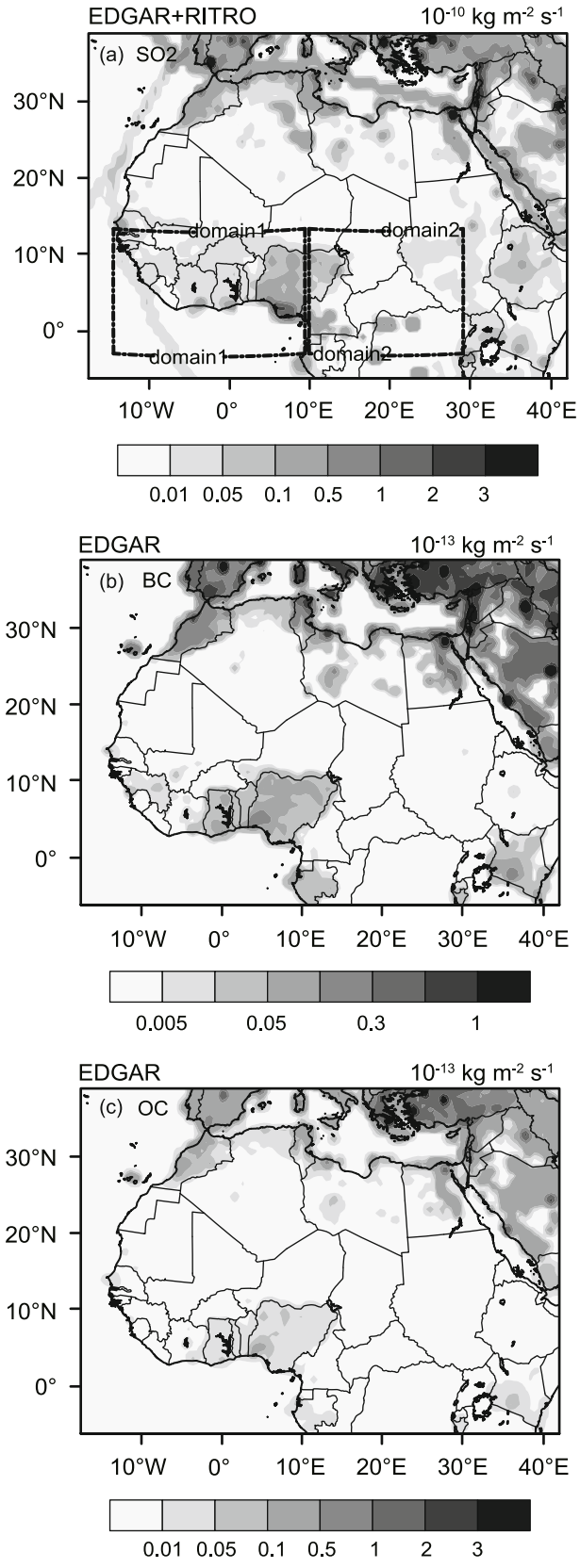

Fig. 2. Emissions rate (units: kg m^{-2} s^{-1}) of (a) $SO_2 \times 10^{-10}$ derived from the EDGAR and RETRO emissions inventories, and (b) $BC \times 10^{-13}$ and (c) $OC \times 10^{-13}$ derived from EDGAR only. The two selected domains are outlined by the dashed black lines in (a): Domain1 is West Africa and Domain2 Central Africa.

the entire simulation domain. The Level-3 Terra/MODIS AOD, retrieved using the Dark-Target (Levy et al., 2007) and Deep Blue (Hsu et al., 2006) aerosol algorithms, is used to evaluate the simulated regional AOD.

We conduct nine sensitivity simulations with varying treatments of the aerosol indirect effect. Four control runs (CTRL, CTRL_BH, CTRL_TC and CTRL_R6) are performed with the different auto-conversion schemes of KS, BH, TC and R6, respectively. In the control simulations, the r_e is constant (at 10 μm) and no aerosol effects are considered. The simulation called "DIRECT" includes the direct effect of all types of aerosols in RegCM4.4.1 (SO_4^{2-}, hydrophobic and hydrophilic OC and BC) with r_e = 10 μm. The first indirect effect of SO_4^{2-}, hydrophilic OC and BC, and the direct effect of all aerosols, are evaluated with the simulation called "INDIR1", in which the size of cloud droplets changes according to the aerosol mass concentration. The effect of the auto-conversion scheme is discussed in section 3.4, and the combined effects of the aerosols (direct, first and second indirect) are included in the runs of "ALL_BH", "ALL_TC" and "ALL_R6" with different auto-conversion schemes. A description of all sensitivity experiments is provided in Table 1.

Here, we focus on the indirect effects of aerosols on the regional climate by changing only the parameterization of the large-scale precipitation processes without changing the convective precipitation parameterizations, because the convective parameterizations implemented in RegCM4.4.1 do not include cloud microphysics that can be directly connected with cloud condensation nuclei and hence aerosols. In addition, we only consider warm cloud processes, as we do not explicitly permit aerosols to act as ice nuclei in these simulations. However, it is possible that the properties of ice cloud can be affected through interaction processes between liquid and ice phases.

3. Results and discussion

3.1. *Control simulations with different auto-conversion parameterizations*

Figures 3a and b show the spatial distributions of the total cloud cover from MODIS and total precipitation from CRU, respectively, over the studied domain during JJA 2006. It can be seen that the cloud and rainfall concentrated in the region south of 15°N, especially in West Africa, are associated with a cloud fraction greater than 80%, and precipitation rates exceeding 200 mm $month^{-1}$ in several regions across Central and West Africa.

First, we examine the influence of changing the auto-conversion scheme on the mean cloud cover and precipitation in the control runs without including the effects of aerosols. The area-averaged values of CLWP, cloud cover (low, medium, high and total), and total precipitation, as well as the ratio of convective to total precipitation, simulated by different control runs with different auto-conversion schemes, are described in Table 2. These mean values are calculated

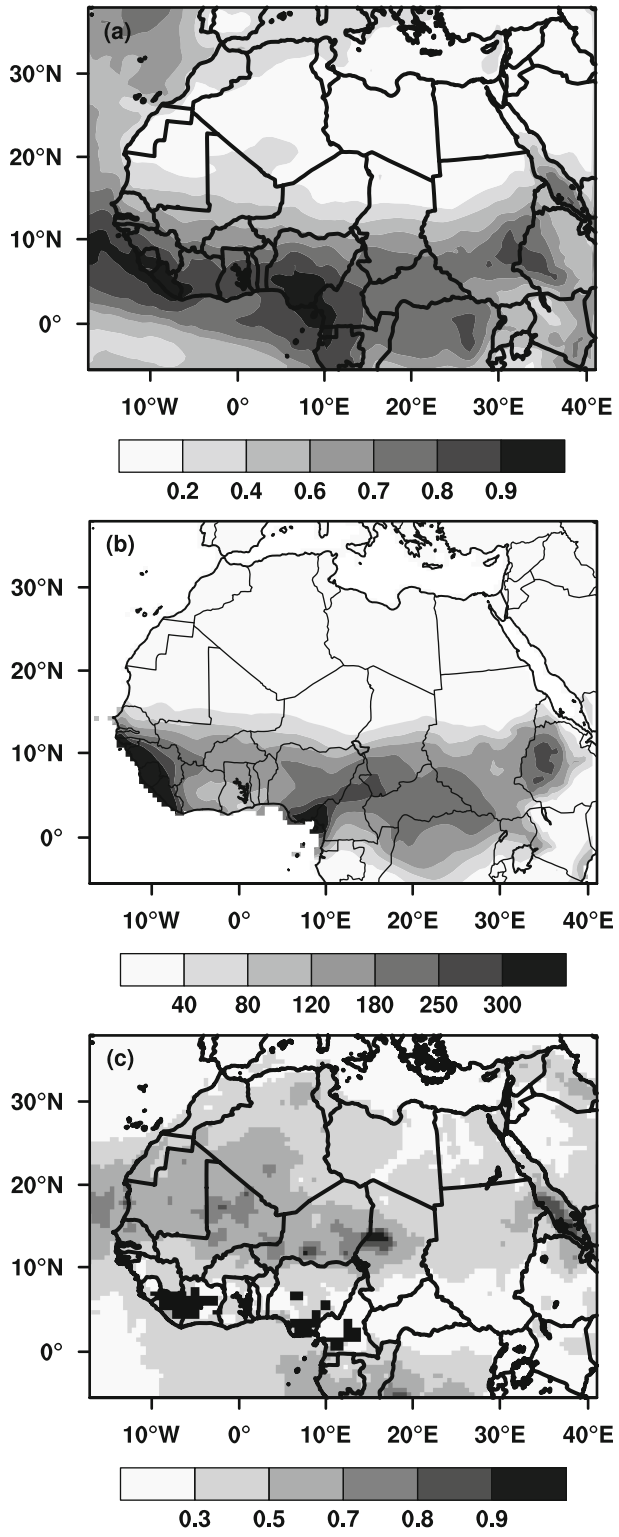

Fig. 3. Spatial distribution of (a) total fractional cloud cover from MODIS/Terra, (b) total precipitation (units: mm month^{-1}) from CRU, and (c) AOD at 550 nm from MODIS/Terra, during JJA 2006.

over West Africa (Domain1) and Central Africa (Domain2) over land only. The CLWP of TC and R6 is greater than that of KS by about 18% and 43%, respectively. This enhancement in cloud liquid water content results in higher values of different cloud types [low (LCLD), medium (MCLD), high (HCLD)] and total cloud, by 18% and 21% for TC and R6, respectively. The surface air temperature (T) averaged over Domain1 with CTRL_R6 and CTRL_TC decreases by approximately 1°C compared to CTRL and CTRL_BH. The CTRL_R6 run produces higher total precipitation (T_{precip}) than CTRL by about 16%. In addition, the ratio of the precipitation produced by convection processes ($C_{\text{precip}}/T_{\text{precip}}$) is over 80% of the total precipitation in all simulations.

In Domain2, the CLWP maximum is produced by the R6 parameterization (CTRL_R6) and the minimum is simulated by the BH parameterization (CTRL_BH). The R6 scheme simulates a larger cloud fraction for all cloud types (LCLD, MCLD, HCLD), and total cloud cover, than the other schemes, with CTRL_R6 resulting in a 25% increase in total cloud with respect to the reference control run (CTRL) (Table 2). Again, CTRL_R6 and CTRL_TC produce lower surface air temperature than CTRL_BH and CTRL. This reduction can be attributed to the increased LCLD in these experiments. These enhancements of CLWP and cloud cover simulated by R6 result in a 10% increase in total precipitation compared to CTRL. It is worth noting here that using different auto-conversion parameterization schemes for large-scale precipitation generally increases the percentage of convective to total precipitation over the two domains compared to the KS scheme. The exception to this is the BH scheme, which reduced this ratio over Domain1, which may be attributable to the enhancement in liquid water content in cloud with the different schemes.

Figure 4a illustrates that, over Domain1, the CTRL, CTRL_BH and CTRL_TC simulations underestimate the total cloud cover compared to MODIS by over 15% with CTRL_BH, while CTRL_R6 overestimates the cloud cover by less than 1%. In addition, over Domain2, the simulations of CTRL, CTRL_BH and CTRL_TC show negative bias (greater than Domain1) compared to MODIS, whereas CTRL_R6 results in lower positive bias than in Domain1.

By comparing the simulated total precipitation based on the control runs with CRU data as shown in Fig. 4b, we find that all the runs result in overestimations, ranging between 30% and 80% with CTRL_BH and CTRL_R6, respectively, over Domain1, and > 50% and > 100% with CTRL_BH and CTRL_R6, respectively, over Domain2.

3.2. *AOD*

The spatial distribution of the AOD over the studied domain during JJA 2006 observed from Terra/MODIS (Dark Target and Deep Blue combined data) at the mid-visible wavelength (550 nm) is shown in Fig. 3c. Here, the AOD from Dark Target and Deep Blue is averaged using the method of Gautam et al. (2011). Higher values of AOD, mainly due to dust, are noted in Central Africa extending to the west. Figure 4c shows the bias in AOD simulated by the five different model sensitivity tests (DIRECT, INDIR1, ALL_BH, ALL_TC, ALL_R6), relative to that detected from Terra/MODIS. We note that these simulations do not include dust emissions; however, these large differences in AOD are

Table 1. List of the experiments performed in this study.

Experiment	Auto-conversion scheme	Aerosols	Effective radius of cloud droplets	Aerosol effect
CTRL	KS	none	Fixed (10 μm)	none
CTRL_BH	BH	none	Fixed (10 μm)	none
CTRL_TC	TC	none	Fixed (10 μm)	none
CTRL_R6	R6	none	Fixed (10 μm)	none
DIRECT	KS	All[1]	Fixed (10 μm)	Direct[2]
INDIR1	KS	All	Predicted	Direct + first indirect[3]
ALL_BH	BH	All	Predicted	Direct + first + second indirect
ALL_TC	TC	All	Predicted	Direct + first + second indirect
ALL_R6	R6	All	Predicted	Direct + first + second indirect

[1]All means (SO_4^{2-} + hydrophobic and hydrophilic OC and BC);
[2]Direct effects, including all simulated aerosols;
[3]First and second indirect effects, including SO_4^{2-} + hydrophilic OC and BC.

Table 2. Mean CLWP (units: g m^{-2}), LCLD, MCLD, HCLD, total cloud cover (TCLD), surface air temperature (T; units: °C), total precipitation (T_{precip}; units: mm $month^{-1}$), and percentage of convective to total precipitation (C_{precip}/T_{precip}), over the West and Central Africa regions (over land only), during JJA 2006, simulated by different control runs (CTRL, CTRL_BH, CTRL_TC, and CTRL_R6) using the different auto-conversion schemes of KS, BH, TC and R6, respectively.

		CTRL	CTRL_BH	CTRL_TC	CTRL_R6
Domain1	CLWP	454.46	402.18	538.14	654.04
	LCLD	0.67	0.68	0.73	0.73
	MCLD	0.41	0.36	0.48	0.58
	HCLD	0.47	0.48	0.76	0.82
	TCLD	0.60	0.61	0.71	0.73
	T	26.05	25.97	25.03	24.69
	T_{precip}	292.75	256.00	278.697	339.674
	C_{precip}/T_{precip}	87.09	85.29	89.65	94.07
Domain2	CLWP	350.36	344.42	395.72	441.28
	LCLD	0.50	0.48	0.51	0.58
	MCLD	0.38	0.41	0.40	0.40
	HCLD	0.41	0.40	0.62	0.72
	TCLD	0.54	0.55	0.64	0.68
	T	26.20	26.57	25.65	24.71
	T_{precip}	249.56	199.78	228.78	275.03
	C_{precip}/T_{precip}	88.89	90.78	91.88	93.96

reduced significantly with the inclusion of the combination of all aerosol effects, especially with using the auto-conversion schemes of R6 and TC, respectively.

3.3. *Aerosol direct and first indirect effects*

Here, we discuss the changes in cloud cover and precipitation due to the aerosol direct and first indirect effects, based on the differences between DIRECT and INDIR1 from the CTRL simulation during JJA 2006. Note that all these three simulations use the same KS auto-conversion scheme, so the differences in the simulations are due primarily to the treatment of the aerosol direct (DIRECT) and first indirect effect (INDIR1).

By focusing on the aerosol effects over Domain1 and Domain2, the results (Table 3) show that, over Domain1, the aerosol direct effect can be linked to a slight suppression in the CLWP. Furthermore, by adding the first indirect effect, this suppression increases to more than −44 g m^{-2}, which is similar to the values published by Costantino and Bréon (2013). Generally, it is found that the CLWP at all atmospheric levels decreases slightly in the direct simulations (generally, < 0.02). The DIRECT run leads to an increase in surface air temperature by 0.2°C relative to CTRL, and this increase enhances in the INDIR1 run.

Over Domain2, the situation is slightly reversed; the aerosol direct effect is also linked to the CLWP, where the CLWP increases (> 1 g m^{-2}). Small changes in LCLD are found relative to CTRL, with a slight increase in the DIRECT run, and reduction of about 0.02, when adding the first indirect effect. Also, the DIRECT simulation results in a reduction of MCLD and HCLD, but the total fractional cover increases; whereas, the INDIR1 simulations suggest an increase corresponding MCLD and a decrease associated HCLD and total cloud cover. Also over Domain2, the INDIR1 run leads to an increase in mean surface temperature by 0.5°C compared to CTRL, but the DIRECT run leads to a

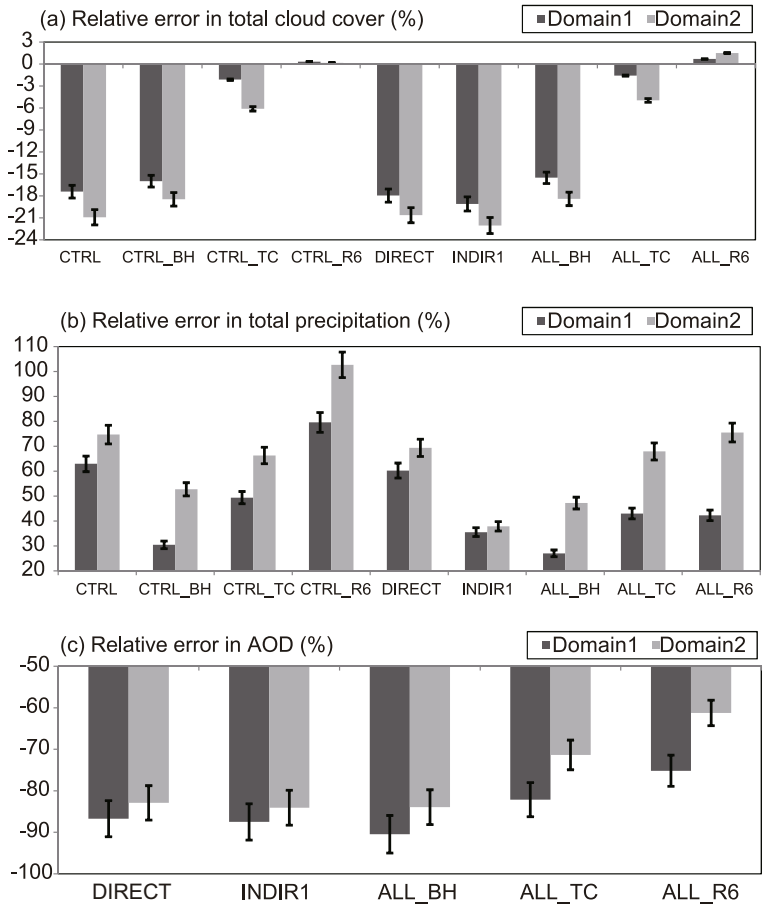

Fig. 4. Relative errors in JJA 2006 (a) total fractional cloud cover and (b) total precipitation (units: %), with respect to MODIS and CRU observations, respectively, for the different simulations, averaged over Domain1 (dark gray) and Domain2 (light gray). The average is calculated over land only. (c) Bias ratio of AOD (units: %) calculated for the simulations with aerosols only, with respect to MODIS. The error bars are plotted at 5%.

Table 3. Differences in mean CLWP (ΔCLWP) (units: g m^{-2}), LCLD (ΔLCLD), MCLD (ΔMCLD), HCLD (ΔHCLD), total cloud cover (ΔTCLD), surface air temperature (ΔT; units: °C), and total precipitation (ΔT_{precip}; units: mm month^{-1}), over the West (Domain1) and Central (Domain2) Africa regions (over land only), during JJA 2006, due to the aerosol direct, first indirect, and the combined aerosols (direct, first and second indirect) effects. These changes are calculated by the difference between the runs of DIRECT and INDIR1 and the control run (CTRL) with auto-conversion scheme of KS; also, between the runs of ALL_BH, ALL_TC and ALL_R6 and their control runs (CTRL_BH, CTRL_TC, and CTRL_R6, respectively).

		DIRECT minus CTRL	INDIR1 minus CTRL	ALL_BH minus CTRL_BH	ALL_TC minus CTRL_TC	ALL_R6 minus CTRL_R6
Domain1	ΔCLWP	−15.92	−44.50	1.16	1.83	0.89
	ΔLCLD	−0.019	−0.021	0.003	0.020	0.065
	ΔMCLD	−0.015	−0.056	−0.008	−0.015	−0.048
	ΔHCLD	−0.007	−0.029	−0.006	0.004	−0.007
	ΔTCLD	−0.004	−0.012	0.003	0.004	0.003
	ΔT	0.19	0.26	−0.11	−0.14	−0.42
	ΔT_{precip}	−8.90	−61.72	−9.28	2.72	−45.55
Domain2	ΔCLWP	01.03	−15.30	−01.98	−03.53	24.63
	ΔLCLD	0.014	−0.023	0.003	0.015	−0.006
	ΔMCLD	−0.005	0.024	−0.006	−0.019	0.046
	ΔHCLD	−0.005	−0.027	−0.001	0.006	−0.003
	ΔTCLD	0.002	−0.008	0.000	0.008	0.009
	ΔT	−00.07	00.52	−00.07	−00.17	−00.15
	ΔT_{precip}	−04.13	−41.98	−05.21	−09.73	−57.11

slightly weaker decrease.

In terms of precipitation changes, results indicate a net reduction in total precipitation over Central Africa in both DIRECT and INDIR1, where ΔP is reduced by 4.0 and 42 mm month^{-1}, respectively. In summary, the reduction in precipitation in West Africa (Domain1) is greater than that in Central Africa (Domain2). This is primarily due to the greater emissions of SO_4^{2-} aerosols over Domain1. SO_4^{2-} aerosols cause a reduction in the r_e, which results in an enhancement of cloud albedo, in turn resulting in enhanced cooling at the surface. It is well known that a cooler surface is associated with suppressed convection processes that reduce the CLWP, in turn reducing the overall precipitation (Lohmann and Feichter, 1997).

3.4. *Combined effects (direct, first and second indirect)*

To study the combined aerosol effects (direct, first and second indirect), we quantify changes in cloud cover and precipitation (as illustrated in Table 3) simulated by ALL_BH, ALL_TC and ALL_R6, relative to their control runs (CTRL_BH, CTRL_TC and CTRL_R6, respectively). With the combined aerosol effects, and consistent with the hypothesis of aerosol inhibition of precipitation (Albrecht, 1989), CLWP is found to increase over West Africa with the three auto-conversion schemes relative to their control runs, with the greatest positive change from the TC scheme (ΔCLWP > 1.8 g m^{-2}) (Table 3). The combined aerosol effects increase the LCLD in all the sensitivity tests, with the greatest change in the R6 scheme (an increase of 0.06). The MCLD reduces consistently across all schemes, with the maximum change in the R6 scheme (0.06); however, there are some differences for HCLD among the different schemes. Whereas the combined aerosol effects reduce the HCLD in BH and R6 (−0.06), the TC scheme shows a slight increase in cloud cover (by 0.004) compared to the cases without aerosols. The mean total cloud cover increase over Domain1 was found to be small, by approximately 0.003, in all schemes. Interestingly, the decrease in air temperature at the surface seen in all experiments, especially ALL_R6 (ΔT = −0.4°C), is a characteristic resulting from the aforementioned overall increase in total cloud cover. The combined aerosol effects suppress the total precipitation over Domain1 with the schemes of BH and R6, with a reduction of precipitation by 46 mm month^{-1} with R6, whereas TC increases the precipitation by less than 3 mm month^{-1}. This increase may be attributable to an enhancement in HCLD.

Over Domain2, the CLWP decreases with the two auto-conversion schemes of BH and TC (ΔCLWP = −2 g m^{-2} and −4 g m^{-2}, respectively), but the R6 scheme causes an increase in CLWP to more than 24 g m^{-2}. The domain-average changes in cloud are relatively small, with the greatest changes for MCLD being an increase of 5% with the R6 scheme. Similar to Domain1, the total cloud cover increases over Domain2 in each experiment, especially for the ALL_TC and ALL_R6 simulations (ΔTCLD > 0.007 and 0.009, respectively), albeit these changes are relatively small. Furthermore, the air temperature, averaged over Domain2, is associated with a decrease in the three experiments relative to their control runs (ΔT = −0.2°C with ALL_TC and ALL_R6). The total precipitation averaged over Central Africa decreases in the three runs with different percentages, with the maximum suppression in the ALL_R6 simulation ($\Delta T_{\text{precip}} > -57\%$) relative to its control run (CTRL_R6).

3.5. *Radiative forcing*

The radiative forcing (RF) of aerosols represents the influence of aerosols on the Earth's energy balance, where a positive RF indicates that the energy of the surface–atmosphere system increases, leading to a warming of the system. In contrast, negative RF corresponds to a cooling of the system. Here, the RF is estimated as the difference in the net radiative flux (downward minus upward) between the present-day total aerosol loading (natural and anthropogenic) and the simulation with no aerosols (control simulations).

The net RF (shortwave and longwave) at the surface and top of the atmosphere (NRF_SRF and NRF_TOA, respectively) due to the different aerosol effects are averaged over Domain1 (Fig. 5a). There is a small positive NRF_SRF over west Africa due to the DIRECT simulation (NRF_SRF = 1 W m^{-2}; standard deviation of ±2.5 W m^{-2}), which becomes negative (−7 W m^{-2}) by including the first indirect effect (INDIR1). Also at the TOA, the warming caused by the direct aerosol effect is transformed to negative RF in the INDIR1 simulation (NRF_TOA = 3 ± 3 W m^{-2} and −8.5 ± 5 W m^{-2}, respectively). The ALL_BH run (combined aerosol effects with the BH scheme) further decreases the cooling at the

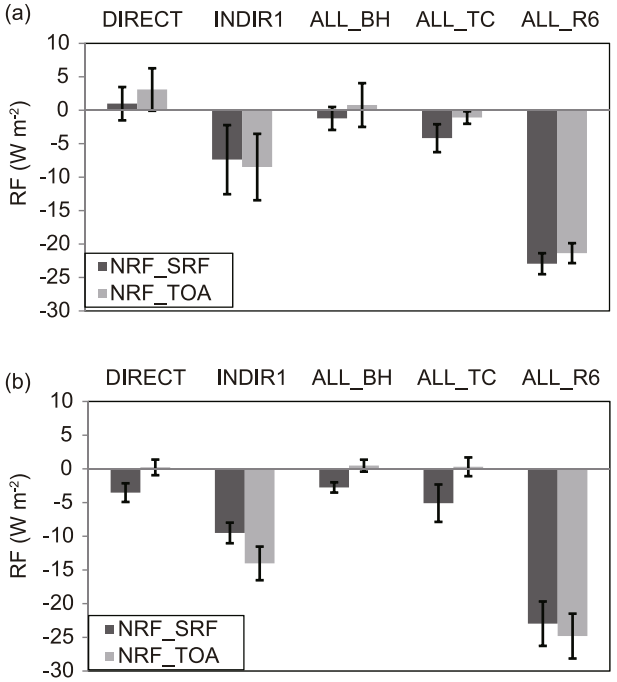

Fig. 5. Net RF (shortwave and longwave) at the surface (dark gray) and TOA (light gray) during JJA 2006 simulated by the different experiments (DIRECT, INDIR1, ALL_BH, ALL_TC, and ALL_R6) averaged over (a) West Africa and (b) Central Africa, with error bars of standard deviation.

surface to -1 ± 2 W m^{-2} and leads to a warming at the TOA of 0.8 ± 3 W m^{-2}. However, using the TC and R6 auto-conversion schemes, the combined aerosol effects (ALL_TC and ALL_R6) lead to a cooling of -4 ± 2 W m^{-2} and -23 ± 2 W m^{-2}, respectively, at the surface, and -1 ± 0.9 W m^{-2} and -21 ± 1.5 W m^{-2}, respectively, at the TOA.

The average NRF_SRF and NRF_TOA over Domain2 are shown in Fig. 5b. The aerosol direct effect (DIRECT) causes negative RF at the surface (-4 ± 1 W m^{-2}) and very low positive RF at the TOA (0.2 ± 1 W m^{-2}). The RF over Domain2 could be due the low emissions of BC and OC over this domain, as shown in the spatial distribution of their emissions in Figs. 2b and c.

After adding the aerosol first indirect effect, the aerosol-induced cooling at the surface is found to be NRF_SRF = -10 ± 2 W m^{-2} and NRF_TOA = -14 ± 3 W m^{-2}, at the surface and TOA, respectively. With the combined aerosol effects, the sign and magnitude of RF differ according to the different auto-conversion schemes, since the three runs keep the cooling at the surface, with the maximum caused by the ALL_R6 run (NRF_SRF = -23 ± 3 W m^{-2}). However, the ALL_BH and ALL_TC runs cause very low warming ($< 0.5 \pm 1$ W m^{-2}) at the TOA, with the ALL_R6 run cooling reaching a large negative forcing of -25 ± 3 W m^{-2}.

3.6. *Influence on WAM circulation*

Here, we investigate the dynamic and thermodynamic responses to the aerosol indirect effect in the cases of the INDIR1 and ALL_R6 simulations, which show pronounced change in precipitation, through analyzing the average WAM circulation anomalies—namely, the changes in the mean SLP (MSLP) and wind field at 850 hPa due to the indirect effect. Figure 6 shows the change in the MSLP and wind field during WAM for both simulations. The continental pressure increases in both schemes but to different degrees. Pressure increases in West Africa and decreases over ocean, which results in a reduction in monsoon pump intensity (Konare et al., 2008). The indirect effects weaken the monsoon's circulation, where the differential wind field has totally reversed its direction (all inflow becomes outflow). ALL_R6 shows a strong reduction in average monsoon circulation (Fig. 6a) compared to the INDIR1 simulation (Fig. 6b). The manifestation of pressure system reduction is shown in the reduction in the wind field.

Intensification of continental pressure is only possible if the atmospheric column has been cooled aloft. This hypothesis can be shown by the analysis of the vertical heating rate owing to latent heat due to convection. Figure 7 shows the vertical zonal average convective heating rate. During JJA, deep convection is inhibited at the middle and high levels of the atmosphere. Comparison between vertical cloud cover (not shown) and the convective heating rate shows that the reduction in vertical cloud extension is due to cooling in the middle and upper levels. Between 5°N and 15°N, the vertical extension of the difference in the convective heating rate shows a dipole structure, where a positive (negative) change in the heating rate is observed in the lower (middle and upper) atmosphere up to 850 hPa (200 hPa). The strength of this dipole is an indication of deep cloud suppression and hence precipitation reduction. The dipole strength is very weak in BH and TC, which agrees with the results in Table 3. The R6 auto-conversion scheme shows a strong reduction in the heating rate (-0.9 K d^{-1}) in the middle and upper troposphere. This reduction in the convective heating rate is comparable to the direct effect made by dust aerosol, as shown in Solmon et al. (2012). On the other hand, the INDIR1 simulation shows a strong yet different signal where the reduction in the convective heating rate has a narrow meridional extension in the

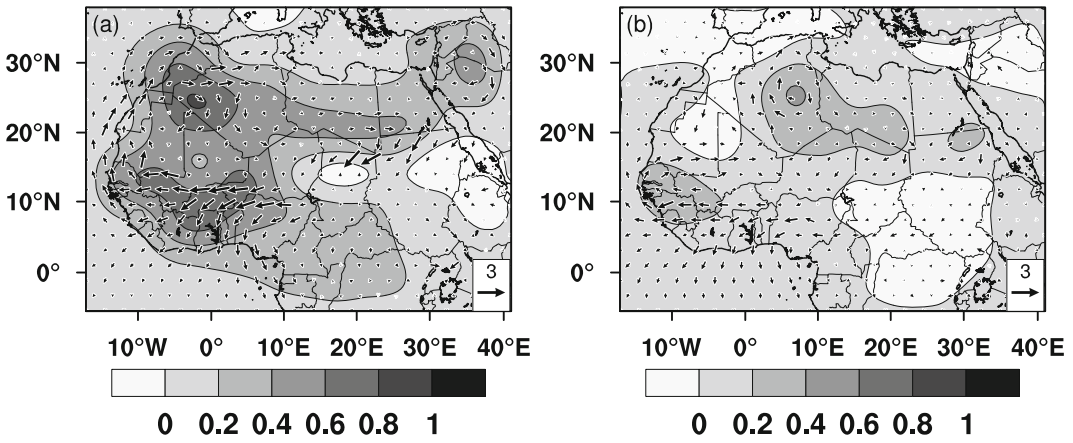

Fig. 6. Effect of the first indirect effect and R6 auto-conversion scheme on monsoon circulation (JJA 2006): (a) difference in circulation between the ALL_R6 and CTRL_R6 simulations at 850 hPa and the MSLP; (b) difference in circulation between the INDIR1 and CTRL simulations at 850 hPa and the MSLP. The shading shows the difference in the MSLP in units of hPa. Dark gray indicates positive anomalies and represents a strengthening of the MSLP, while the lightest gray shows below-zero anomalies and presents a weakening of the MSLP. Arrows represents the difference in circulation, i.e., the direction and relative intensity of the change in the wind field (units: m s^{-1}) due to the auto-conversion.

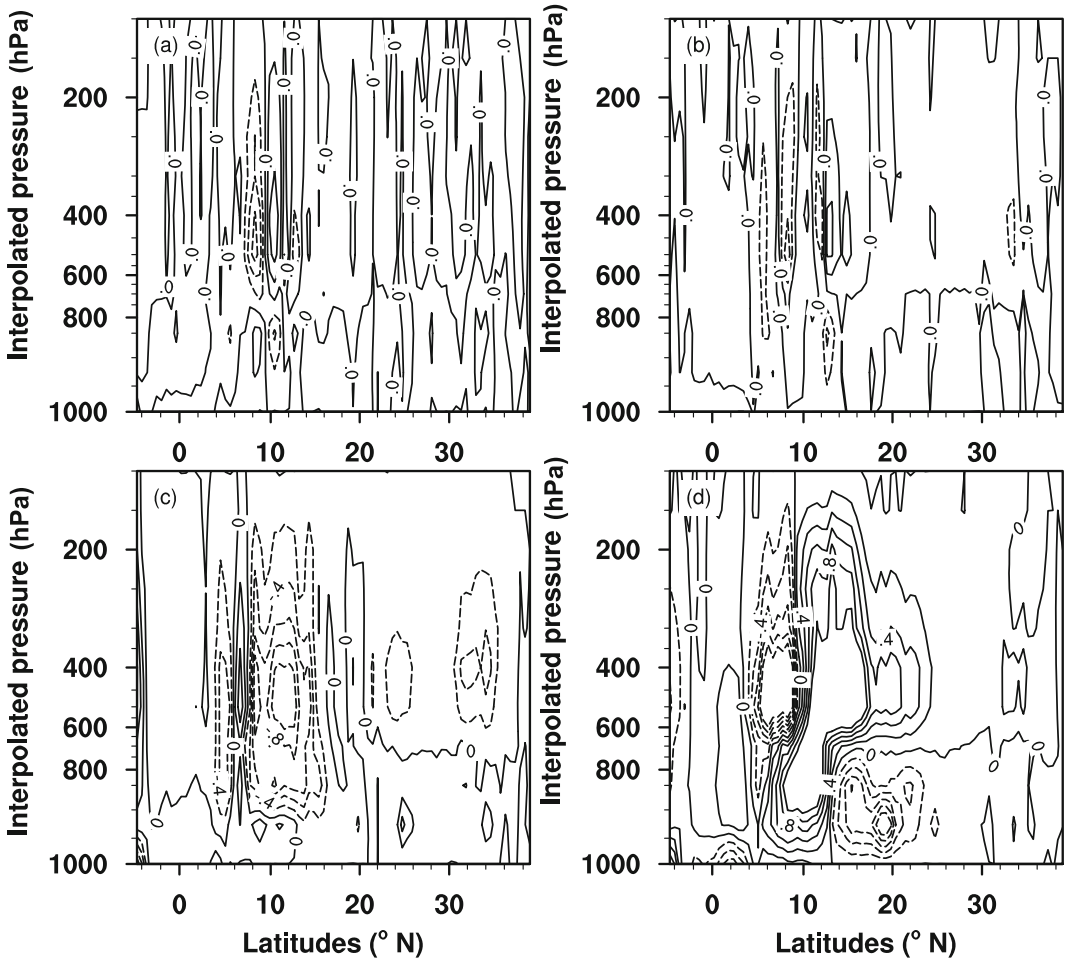

Fig. 7. Effects of aerosols on convection with the different auto-conversion schemes. Specifically, the panels show meridional cross sections of the heating rate due to convection (units: K d^{-1}), where negative in dashed lines (positive in solid lines) values indicate cooling (heating) of the atmosphere: (a) ALL_BH minus CTRL_BH; (b) ALL_TC minus CTRL_TC; (c) ALL_R6 minus CTRL_R6; (d) the INDIR1 minus CTRL.

middle troposphere and, contrary to R6, the positive convective heating rate extends to the upper troposphere but north of 10°N. The first indirect effect reduces the CLWP, leading to a reduction in LCLD and yet enhances cloud albedo. This pathway results in a reduction in MCLD and a stabilization of the atmospheric column. On the other pathway of the ALL_R6 that increases the low cloud cover, which results in reduction in surface temperature, which in turn reduces monsoon circulation and inhibits deep convection.

4. Summary and conclusion

In this work, we study the aerosol direct and indirect effects on the climate of tropical Africa, focusing on the western and central regions during the summer season of the WAM, using RegCM4.4.1 implemented with three precipitation auto-conversion schemes (BH, TC, and R6).

We find that, at low cloud liquid water mixing ratios with relatively larger cloud droplets (r_e = 10 μm) or low aerosol concentrations, the auto-conversion rate is accelerated by the BH scheme, more so than in the TC, R6 and KS schemes, respectively, when the f_c is less than or equal to 50%. However, as the cloud cover increases and reaches closer to 100%, the BH and KS schemes produce less precipitation than the other two schemes. Whereas, for extremely low in-cloud liquid water ($q_L \leqslant 0.1$ g kg^{-1}) with smaller cloud droplets (r_e = 7.5 μm) or high aerosol concentrations, the TC and BH schemes (with $f_c \leqslant 50\%$) result in larger precipitation than the other schemes. Based on these detailed sensitivity simulations, we note the importance of the implementation of aerosol properties (as the r_e) in the parameterization of the auto-conversion process, which can alter the precipitation rates in the model (as in the cases of the first indirect and the combined aerosol effects with the different auto-conversion schemes).

The inclusion of both the aerosol direct and first indirect effects leads to cooling at both the surface and the TOA, which results in suppression of precipitation over West and Central Africa. The sign and magnitude of the RF of the combined aerosol effects (direct, first and second indirect) are influenced by the different auto-conversion schemes. At the surface, the various schemes result in negative net RF, with maximum values exceeding −20 W m^{-2}, attaining its largest reduction with the R6 scheme over West and Central Africa. Whereas, at the TOA, the difference in the sign of RF be-

tween the three schemes is more obvious, since the BH and TC schemes cause a slight warming of the order of +1 W m^{-2} over the central domain, and cooling over the western domain (−2 W m^{-2}). However, the R6 scheme results in cooling over both regions by less than −20 W m^{-2}. Our simulations show that the precipitation in West and Central Africa, during the WAM period, is likely to be highly sensitive to the parameterization or treatment of the indirect effect in models, and the inclusion of aerosol indirect effects helps significantly in improving the agreement between measurements and model results.

Finally, the analysis of the average WAM circulation and convective heating rate under the influence of aerosols shows that the first indirect effect and R6 scheme weaken the WAM main circulation, which in turn suppresses precipitation due to two different pathways.

Acknowledgements. The authors would like to thank both of the NOAA/OAR/ESRL PSD, Boulder, Colorado, USA, for providing the NCEP_Reanalysis 2 data on their web site at http://www.esrl.noaa.gov/psd/, and ICTP on their website at http://clima-dods.ictp.it/data/regcm4/NNRP2/.

REFERENCES

Albrecht, B. A., 1989: Aerosols, cloud microphysics, and fractional cloudiness. *Science*, **245**, 1227–1230, https://doi.org/10.1126/science.245.4923.1227.

Beheng, K. D., 1994: A parameterization of warm cloud microphysical conversion processes. *Atmo. Res.*, **33**, 193–206, https://doi.org/10.1016/0169-8095(94)90020-5.

Chiapello, I., C. Moulin, and J. M. Prospero, 2005: Understanding the long-term variability of African dust transport across the Atlantic as recorded in both Barbados surface concentrations and large-scale total ozone mapping spectrometer (TOMS) optical thickness. *J. Geophys. Res.*, **110**, D18S10, https://doi.org/10.1029/2004JD005132.

Costantino, L., and F. M. Bréon, 2013: Aerosol indirect effect on warm clouds over South-East Atlantic, from co-located MODIS and CALIPSO observations. *Atmospheric Chemistry and Physics*, **13**, 69–88, https://doi.org/10.5194/acp-13-69-2013.

Dickinson, R. E., Henderson-Sellers, A., and P. J. Kennedy, 1993: Biosphere-atmosphere transfer scheme (BATS) version 1e as coupled to the NCAR community climate model. National Center for Atmospheric Research Technical Note NCAR. TN-387+STR, 72 pp.

Emmons, L. K., and Coauthors, 2010: Description and evaluation of the Model for Ozone and Related chemical Tracers, version 4 (MOZART-4). *Geoscientific Model Development*, **3**, 43–67, https://doi.org/10.5194/gmd-3-43-2010.

Fan, J. W., Y. Wang, D. Rosenfeld, and X. H. Liu, 2016: Review of aerosol-cloud interactions: Mechanisms, significance, and challenges. *J. Atmos. Sci.*, **73**, 4221–4252, https://doi.org/10.1175/JAS-D-16-0037.1.

Fritsch, J. M., and C. F. Chappell, 1980: Numerical prediction of convectively driven mesoscale pressure systems. Part 1: Convective parameterization. *J. Atmos. Sci.*, **37**, 1722–1733, https://doi.org/10.1175/1520-0469(1980)037<1722:NPOCDM>2.0.CO;2.

Gautam, R., and Coauthors, 2011: Accumulation of aerosols over the Indo-Gangetic plains and southern slopes of the Himalayas: Distribution, properties and radiative effects during the 2009 pre-monsoon season. *Atmos. Chem. Phys.*, **11**, 12 841–12 863, https://doi.org/10.5194/acp-11-12841-2011.

Giorgi, F., 1989: Two-dimensional simulations of possible mesoscale effects of nuclear war fires. I: Model description. *J. Geophys. Res.*, **94**, 1127–1144, https://doi.org/10.1029/JD094iD01p01127.

Giorgi, F., and W. L. Chameides, 1986: Rainout lifetimes of highly soluble aerosols and gases as inferred from simulations with a general circulation model. *J. Geophys. Res.,* **91**, 14 367–14 376, https://doi.org/10.1029/JD091iD13p14367.

Giorgi, F., and Coauthors, 2012: RegCM4: Model description and preliminary tests over multiple CORDEX domains. *Climate Research*, **52**, 7–29, https://doi.org/10.3354/cr01018.

Giorgi, F., M. R. Marinucci, and G. T. Bates, 1993: Development of a second-generation regional climate model (RegCM2). Part I: Boundary-layer and radiative transfer processes. *Mon. Wea. Rev.*, **121**, 2794–2813, https://doi.org/10.1175/1520-0493(1993)121<2794:DOASGR>2.0.CO;2.

Grell, G. A, 1993: Prognostic evaluation of assumptions used by cumulus parameterizations. *Mon. Wea. Rev*., **121**, 764–787, https://doi.org/10.1175/1520-0493(1993)121<0764:PEOAUB>2.0.CO;2.

Gu, Y., K. N. Liou, J. H. Jiang, H. Su, and X. Liu, 2012: Dust aerosol impact on North Africa climate: A GCM investigation of aerosol-cloud-radiation interactions using A-Train satellite data. *Atmos. Chem. Phy. Discuss.*, **11**, 1667–1679, https://doi.10.5194/acpd-11-31401-2011.

Gu, Y., K. N. Liou, Y. Xue, C. R. Mechoso, W. Li, and Y. Luo, 2006: Climatic effects of different aerosol types in China simulated by the UCLA general circulation model. *J. Geophys. Res.*, **111**, D15201, https://doi.org/10.1029/2005 JD006312.

Gultepe, I., and G. A. Isaac, 1997: Liquid water content and temperature relationship from aircraft observations and its applicability to GCMs. *J. Climate*, **10**, 446–452, https://doi.org/10.1175/1520-0442(1997)010<0446:LWCATR>2.0.CO;2.

Hegg, D. A., 1994: Cloud condensation nucleus-sulphate mass relationship and cloud albedo. *J. Geophys. Res.*, **99**, 25 903–25 907, https://doi.org/10.1029/94JD02224.

Holtslag, A. A. M., E. I. F. de Bruijn, and H. L. Pan, 1990: A high resolution air mass transformation model for short-range weather forecasting. *Mon. Wea. Rev.*, **118**, 1561–1575, https://doi.org/10.1175/1520-0493(1990)118<1561:AHRAMT>2.0.CO;2.

Hsu, N. C., S. C. Tsay, M. D. King, and J. R. Herman, 2006: Deep blue retrievals of Asian aerosol properties during ACE-Asia. *IEEE Trans. Geosci. Remote Sens.*, **44**, 3180–3195, https://doi.org/10.1109/TGRS.2006.879540.

Huang, J. F., C. D. Zhang, and J. M. Prospero, 2009: African aerosol and large-scale precipitation variability over West Africa. *Environ. Res. Lett.*, **4**, 015006, https://doi.org/10.1088/1748-9326/4/1/015006.

Huang, Y., 2005: Assessments of the direct and indirect effects of anthropogenic aerosols on regional precipitation over east Asia using a coupled regional climate-chemistry-aerosol model. PhD dissertation, Georgia Institute of Technology.

Huang, Y., W. L. Chameides, and R. E. Dickinson, 2007: Direct and indirect effects of anthropogenic aerosols on regional precipitation over east Asia. *J. Geophys. Res.*, **112**, D03212,

https://doi.org/10.1029/2006JD007114.

IPCC, 2013: *Climate Change 2013: The Physical Science Basis. Contribution of Working Group I to the Fifth Assessment Report of the Intergovernmental Panel on Climate Change*. Cambridge University Press, 1535 pp.

Ji, Z. M., G. L. Wang, J. S. Pal, and M. Yu, 2016: Potential climate effect of mineral aerosols over West Africa. Part I: Model validation and contemporary climate evaluation. *Climate Dyn.*, **46**, 1223–1239, https://doi.org/10.1007/s00382-015-2641-y.

Kessler, E., 1969: On the distribution and continuity of water substance in atmospheric circulations. *Meteorological Monographs*. Vol. 10, American Meteorological Society, 84 pp, https://doi.org/10.1007/978-1-935704-36-2_1.

Kiehl, J. T., J. J. Hack, G. B. Bonan, B. A. Boville, B. P. Briegleb, D. L. Williamson, and P. J. Rasch, 1996: Description of the NCAR community climate model (CCM3). Technical Report NCAR/TN-420+STR.

Kim, K. M., W. K. M. Lau, Y. C. Sud, and G. K. Walker, 2010: Influence of aerosol-radiative forcings on the diurnal and seasonal cycles of rainfall over West Africa and Eastern Atlantic Ocean using GCM simulations. *Climate Dyn*., **35**(1), 115–126, https://doi.org/10.1007/s00382-010-0750-1.

Kodros, J. K., C. E. Scott, S. C. Farina, Y. H. Lee, C. L'Orange, J. Volckens, and J. R. Pierce 2015: Uncertainties in global aerosols and climate effects due to biofuel emissions, *Atmos. Chem. Phys*., **15**, 8577–8596, https://doi.org/10.5194/acp-15-8577-2015.

Konare, A., A. S. Zakey, F. Solmon, F. Giorgi, S. Rauscher, S. Ibrah, and X. Bi, 2008: A regional climate modeling study of the effect of desert dust on the West African monsoon. *J Geophys. Res*., **113**: D12206, https://doi.org/10.1029/2007JD009322.

Levy, R. C., L. A. Remer, S. Mattoo, E. F. Vermote, and Y. J. Kaufman, 2007: Second-generation operational algorithm: Retrieval of aerosol properties over land from inversion of Moderate Resolution Imaging Spectroradiometer spectral reflectance. *J. Geophys. Res.*, **112**, D13211, https://doi.org/10.1029/2006JD007811.

Liu, Y. G., and P. H. Daum, 2004: Parameterization of the autoconversion process. Part I: Analytical formulation of the Kessler-type parameterizations. *J. Atmos. Sci.*, **61**, 1539–1548, https://doi.org/10.1175/1520-0469(2004)061<1539:POTAPI>2.0.CO;2.

Liu, Y. G., P. H. Daum, and R. McGraw, 2004: An analytical expression for predicting the critical radius in the autoconversion parameterization. *Geophys. Res. Lett.*, **31**, L06121, https://doi.org/10.1029/2003GL019117.

Liu, Y. G., P. H. Daum, R. L. McGraw, M. A. Miller, and S. J. Niu, 2007: Theoretical expression for the autoconversion rate of the cloud droplet number concentration. *Geophys. Res. Lett.*, **34**, L16821, https://doi.org/10.1029/2007GL030389.

Lohmann, U., and J. Feichter, 1997: Impact of sulfate aerosols on albedo and lifetime of clouds: A sensitivity study with the ECHAM4 GCM. *J. Geophys. Res.*, **102**, 13 685–13 700, https://doi.org/10.1029/97JD00631.

Martin, G. M., D. W. Johnson, and A. Spice, 1994: The measurement and parameterization of effective radius of droplets in warm stratocumulus clouds. *J. Atmos. Sci.*, **51**, 1823–1842, https://doi.org/10.1175/1520-0469(1994)051<1823:TMAPOE>2.0.CO;2.

Mitchell, T. D., and P. D. Jones, 2005: An improved method of constructing a database of monthly climate observations and associated high-resolution grids. *International Journal of Climatology*, **25**(6), 693–712, https://doi.org/10.1002/joc.1181.

Olivier, J. G. J., J. J. M. Berdowski, J. A. H. W. Peters, J. Bakker, A. J. H. Visschedijk, and J.-P. J. Bloos, 2001: Applications of EDGAR. Including a description of EDGAR 3.0: Reference database with trend data for 1970-1995. RIVM, Bilthoven. RIVM report no. 773301 001/NOP report no. 410200 051.

Pal, J. S., E. E. Small, and E. A. B. Eltahir, 2000: Simulation of regional-scale water and energy budgets: Representation of subgrid cloud and precipitation processes within RegCM. *J. Geophys. Res.*, **105**, 29 579–29 594, https://doi.org/10.1029/2000JD900415.

Pruppacher, H. R., and J. D. Klett, 1997: *Microphysics of Clouds and Precipitation*. 2nd ed., Springer, 954 pp.

Qian, Y., and F. Giorgi, 1999: Interactive coupling of regional climate and sulfate aerosol models over eastern Asia. *J. Geophys. Res.*, **104**, 6477–6499, https://doi.org/10.1029/98JD02347.

Rogers, R. R., and M. K. Yau, 1989: *A Short Course in Cloud Physics*. 3rd ed., Oxford, Pergamon, UK.

Rotstayn, L. D., and Y. G. Liu, 2005: A smaller global estimate of the second indirect aerosol effect. *Geophys. Res. Lett.*, **32**, L05708, https://doi.org/10.1029/2004GL021922.

Schultz, M. G., and Coauthors, 2007: REanalysis of the TROpospheric chemical composition over the past 40 years—A long-term global modeling study of tropospheric chemistry funded under the 5th EU Framework Programme 2007. Technical Report, EU-Contract No. EVK2-CT-2002-00170, 20 pp. [Available online at http://retro.enes.org/reports/D1–6_final.pdf]

Seinfeld, J. H., and S. N. Pandis, 2006: *Atmospheric Chemistry and Physics: From Air Pollution to Climate Change*. 2nd ed., Wiley-Interscience.

Solmon, F., F. Giorgi, and C. Liousse, 2006: Aerosol modelling for regional climate studies: Application to anthropogenic particles and evaluation over a European/African domain. *Tellus*, **58B**, 51–72, https://doi.org/10.1111/j.1600-0889.2005.00155.x.

Solmon, F., N. Elguindi, and M. Mallet, 2012: Radiative and climatic effects of dust over West Africa, as simulated by a regional climate model. *Climate Research*, **52**, 97–113, https://doi.org/10.3354/cr01039.

Sylla, M. B., E. Coppola, L. Mariotti, F. Giorgi, P. M. Ruti, A. Dell'Aquila, and X. Bi, 2010: Multiyear simulation of the african climate using a regional climate model (RegCM3) with the high resolution ERA-interim reanalysis. *Climate Dyn.*, **35**, 231–274, https://doi.org/10.1007/s00382-009-0613-9.

Tripoli, G. J., and W. R. Cotton, 1980: A numerical investigation of several factors contributing to the observed variable intensity of deep convection over South Florida. *J. Atmos. Sci.*, **19**, 1037–1063, https://doi.org/10.1175/1520-0450(1980)019<1037:ANIOSF>2.0.CO;2.

Twomey, S., 1977: The influence of pollution on the shortwave albedo of clouds. *J. Atmos. Sci.*, **34**, 1149–1152, https://doi.org/10.1175/1520-0469(1977)034<1149:TIOPOT>2.0.CO;2.